Performance Analysis of RF Energy Harvesting Mobile Edge Computing Network Using NOMA Scheme with Dual Access Points

Minh-Thong Vo[1,2(✉)], Thanh-Nam Nguyen[1,2], Van-Truong Truong[1,2], and Dac-Binh Ha[1,2]

[1] Faculty of Electrical-Electronic Engineering, Duy Tan University, Da Nang 550000, Vietnam
{nguyenthanhnam9,truongvantruong}@dtu.edu.vn, hadacbinh@duytan.edu.vn
[2] Institute of Research and Development, Duy Tan University, Da Nang 550000, Vietnam
vominhthong@dtu.edu.vn

Abstract. Mobile edge computing (MEC) is an emerging cloud computing trend that enables terminal users with limited computing ability to offload their tasks to the edge servers. In this paper, we study the performance of the MEC system using non-orthogonal multiple access (NOMA) and radio frequency energy harvesting techniques (RF EH). Specifically, a user harvests energy from a hybrid access point (HAP) and offloads tasks to the edge servers using the NOMA scheme over wireless channels. The protocol, specifically NOMA-MEC, is proposed for this considered system, and the closed-form expression of successful computation probability (SCP) is derived to evaluate the system performance. In addition, an OMA-based reference protocol, namely OMA-MEC, was used to compare with the proposed solution. The numerical results show the superior performance of NOMA-MEC over OMA-MEC in terms of SCP. Furthermore, system behaviors were clarified by investigating SCP using Monte-Carlo simulation through critical parameters such as time switching ratio, power allocation coefficient, task length, and transmit power.

Keywords: mobile edge computing · non-orthogonal multiple access · uplink NOMA · successful computation probability · multiple devices

1 Introduction

In recent decades, Cloud computing (CC) has provided resources such as software, services, and hardware to terminal users (TU) through the Internet. CC allows TUs to conveniently access any resource in the cloud (i.e., server) anytime and anywhere [1]. However, with the development of autonomous systems that require real-time processing, such as industrial IoT networks, and V2X networks,

N.-S. Vo and H.-A. Tran (Eds.): INISCOM 2023, LNICST 531, pp. 75–88, 2023.
https://doi.org/10.1007/978-3-031-47359-3_6

CC no longer fulfills some of the new requirements of TUs [2,3]. Mobile edge computing (MEC) networks are designed and deployed with proximity wireless servers to assist TUs in addressing real-time demanding tasks [4]. In the MEC paradigm, the computing and IT services are provided at the network edge, closest to the MEC devices. They can be smartphones, set-top boxes, IoT devices, or sensor and actuator nodes [5]. MEC can be seen as the next generation of evolution in the field of CC, helping to meet the higher requirements of TUs, especially real-time requirements. MEC ensures low latency, instant response, saves bandwidth, increases security, and good scalability [6].

Currently, the non-orthogonal multiple access (NOMA) technique is applied in MEC networks to solve the problems of many users, high communication data rate requirements, and low latency [7]. NOMA allows multi-user communications through a non-orthogonal division multiplexing technique in which TUs are distinguished based on power level. Obviously, the combination of MEC and NOMA significantly enhances the TU experience and network performance. NOMA provides outstanding advantages in improving spectrum efficiency and throughput, while MEC allows for improved overall network performance. Furthermore, MEC can widely distribute computing resources from the centralized cloud to the network's edge and immediately serve TUs. The NOMA MEC network has been proven effective in enhancing performance compared to OMA-based systems [8].

A radio frequency energy harvesting technique is used to enhance the performance of the MEC-based system further, allowing the TUs to collect energy from RF electromagnetic waves in the wireless environment to operate [9]. In this context, TUs can collect energy from power stations or hybrid access points (HAPs), thus prolonging network connectivity. Integrating these technologies in future wireless communication systems could significantly improve network performance by taking advantage of their strengths [10,11]. For instance, in the work [12], the authors investigate the MEC network using NOMA and RF EH with the power station. Specifically, the user collects radio energy from the power station and offloads the tasks to the edge servers using the NOMA technique to the two access points (APs). To the best of our knowledge, no studies have investigated the MEC network model with mixed APs combined with NOMA offloading. The main contributions of this study are as follows:

- Propose a MEC network model based on the NOMA technique and RF EH transmission from mixed APs, i.e., AP and HAP operating together in the system.
- Propose a four-phase operation protocol, namely NOMA-MEC, for the proposed system that allows radio energy transmission and offloading. In addition, an OMA-based reference protocol, namely OMA-MEC, is analyzed to clarify system performance.
- Derive the close-form expressions of the successful calculation probability (SCP) of NOMA-MEC and OMA-MEC protocol to evaluate the performance of the proposed system.

– Investigate the behavior of the proposed system according to the main parameters such as signal-to-noise ratio, time switching ratio, power allocation coefficient, and task division ratio.

The paper's layout is as follows: Section 2 presents the system model and communication protocol. Section 3 presents the performance analysis of the proposed model. Section 4 describes the numerical results. And Sect. 5 is the conclusion and future scope of the paper.

2 System Model and Communication Protocol

In this study, we investigate the RF EH NOMA MEC network system as depicted in Fig. 1. The network model consists of a user device (U) and two access points, including a hybrid access point (HAP) and a common access point (AP). Suppose the HAP can provide the RF power and offloading services to U, while the AP only provides the offloading services. The devices are equipped with a single antenna and operate in half-duplex mode. The system operates over Rayleigh fading channel.

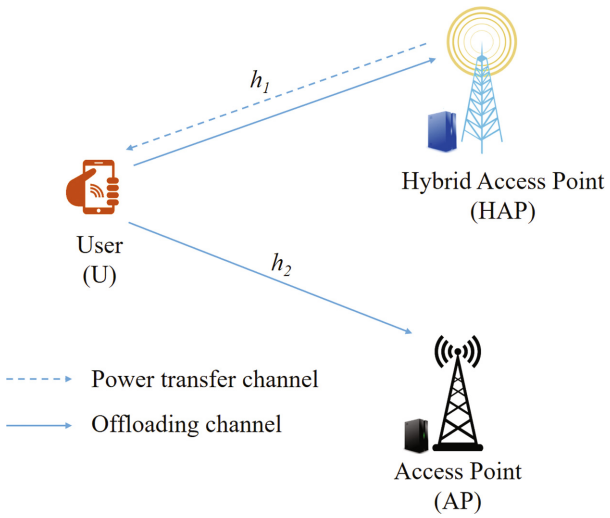

Fig. 1. System model for RF EH NOMA MEC with dual APs system

Assume that U consistently performs tasks of length L bits. Each task consists of two parts: the first L_1-bit part is designed to offload the HAP, and the second L_2-bit part reduces the load on the AP ($L_1 + L_2 = L$). Furthermore, due to the situation of limited power, U offloads its tasks by using all the energy obtained from the HAP and adopting the downlink NOMA technique. Finally, the HAP and AP feedback on the computation results to U using the uplink NOMA

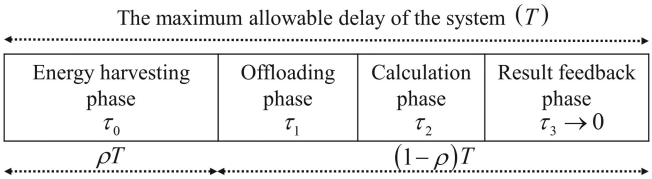

Fig. 2. Time flow chart for proposed system.

technique. This protocol, called NOMA-MEC, can be divided into four phases, as shown in the time flow diagram in Fig. 2.

We continue to present NOMA-MEC protocol for the proposed system with specific mathematical expressions as follows.

Phase 1- Energy Harvesting Phase: In this phase, U collects radio energy from the HAP in the time interval $\tau_0 = \rho T$, where ρ is the time switching ratio, $0 < \rho < 1$, and T is the block time allocated to the system or the maximum allowable delay of the system. The energy obtained by U in this phase is as follow:

$$E_U = \eta P_0 g_1 \rho T, \tag{1}$$

where η is the energy conversion factor, $0 < \eta \leq 1$; P_0 is the transmit power of the HAP; g_1 is the channel power gain from U to the HAP.

Phase 2- Offloading Phase: During this phase, U uses all the energy collected in **Phase 1** to simultaneously offload tasks to the HAP and AP using the downlink NOMA. According to NOMA technique, U transmit the superimposed signal as follows:

$$x = \sqrt{a}x_1 + \sqrt{1-a}x_2. \tag{2}$$

where x_1 and x_2 are L_1-bit and L_2-bit tasks respectively; a is the power allocation coefficient. Thus, the received signal at the HAP is as follow:

$$y_{HAP}^{NOMA-MEC} = h_1\sqrt{P_t}x + n_1 = h_1\sqrt{P_t}(\sqrt{a}x_1 + \sqrt{1-a}x_2) + n_1, \tag{3}$$

where, h_1 is the channel coefficient from U to HAP, n_1 is the additive white Gaussian noise (AWGN) of the U-HAP channel. Following that, the transmit power of U is:

$$P_t = \frac{E_U}{(1-\rho)T - \tau_2} = bP_0 g_1, \tag{4}$$

where $b \triangleq \frac{\eta\rho T}{(1-\rho)T-\tau_2}$; τ_2 is the maximum computation time at the MEC servers and is calculated by

$$\tau_2 = \max\left\{\frac{\delta_1 L_1}{f_1}, \frac{\delta_2 L_2}{f_2}\right\}, \tag{5}$$

where δ_X $(X \in \{1,2\})$ is the number of CPU cycles required to process one input bit; f_X $(X \in \{1,2\})$ denoted the server CPU frequency at the HAP and AP, respectively.

Similarly, the received signal at the AP is as follow:

$$y_{\mathrm{AP}}^{NOMA-MEC} = h_2\sqrt{P_t}(\sqrt{a}x_1 + \sqrt{1-a}x_2) + n_2, \tag{6}$$

where, h_2 is the channel coefficient from U to HAP, n_2 is the AWGN of the U-AP channel.

Phase 3- Calculation Phase: In this phase, assuming HAP is located closer to U than AP, thus that HAP can directly decode to get x_1 while AP uses successive interference cancelation (SIC) to decode signal x_1 first and then subtract x_1 to get x_2 signal [10,13]. Hence, the signal-to-interference noise ratio (SINR) at the HAP is as follow:

$$\gamma_1 = \frac{aP_t|h_1|^2}{(1-a)P_t|h_1|^2 + N_0} = \frac{ab\gamma_0 g_1^2}{(1-a)b\gamma_0 g_1^2 + 1}, \tag{7}$$

where $\gamma_0 = \frac{P_0}{N_0}$.

The SINR and signal-to-noise ratio (SNR) at the AP to decode x_1 and x_2 signals are:

$$\gamma_2^{x_1} = \frac{ab\gamma_0 g_1 g_2}{(1-a)b\gamma_0 g_1 g_2 + 1}, \tag{8}$$

$$\gamma_2^{x_2} = (1-a)b\gamma_0 g_1 g_2, \tag{9}$$

The capacity of U-HAP and U-AP channels is calculated according to Shannon's theorem as follows:

$$C_1 = (1-\rho)B\log_2(1+\gamma_1), \tag{10}$$

$$C_2 = (1-\rho)B\log_2(1+\gamma_2^{x_2}), \tag{11}$$

where B is the bandwidth.

The offloading time when U offloads its task to HAP and AP is calculated as follows:

$$t_1 = \frac{L_1}{C_1} = \frac{L_1}{(1-\rho)B\log_2(1+\gamma_1)}, \tag{12}$$

$$t_2 = \frac{L_2}{C_2} = \frac{L_2}{(1-\rho)B\log_2(1+\gamma_2^{x_2})}. \tag{13}$$

The maximum offload time τ of this system is:

$$\tau = \max\left\{t_1 + \frac{\delta_1 L_1}{f_1}, t_2 + \frac{\delta_2 L_2}{f_2}\right\}. \tag{14}$$

Phase 4- Result Feedback Phase: In this phase, U receives calculation results from HAP and AP in time τ_3. τ_3 is very small compared to transmission and computation time, so it can be ignored [8,10].

The power gain of the Rayleigh fading channel g_i follows an exponential distribution with the parameter $\lambda_i,\ i \in \{1,2\}$. Therefore, the cumulative distribution function (CDF) and the probability density function (PDF) of g_i are given by following equations.

$$F_{g_i}(x) = 1 - e^{-\frac{x}{\lambda_i}}, \tag{15}$$

$$f_{g_i}(x) = \frac{1}{\lambda_i} e^{-\frac{x}{\lambda_i}}. \tag{16}$$

3 Performance Analysis

In this section, we analyze the RF EH NOMA-MEC with mixed APs system performance through the criterion of SCP, denoted by Φ_s. It is the probability that all tasks are completed within the maximum allowable delay time $T > 0$. Accordingly, Φ_s is given by the formula:

$$\Phi_s = \Pr\left(\tau < (1-\rho)T\right). \tag{17}$$

To evaluate the system performance, we find the following theorem.

Theorem 1. *The approximation close-form expression of the SCP of the proposed system under NOMA-MEC protocol, denoted by Φ_s^{NOMA}, over Rayleigh fading channel is as follow:*

$$\Phi_s^{NOMA} = \begin{cases} 0, & \text{if } \frac{a}{1-a} \le 2^{\frac{L_1}{(1-\rho)B\Omega_1}} - 1 \\ \frac{\pi e^{-\sqrt{\beta_1}}}{2Q\lambda_1} \sum\limits_{q=1}^{Q} t_q^{\frac{1}{\lambda_1}-1} e^{\frac{\beta_2}{\lambda_2 \ln t_q}} \sqrt{1-x_q^2}, & \text{if } \frac{a}{1-a} > 2^{\frac{L_1}{(1-\rho)B\Omega_1}} - 1 \end{cases} \tag{18}$$

where $\beta_1 = \frac{2^{\frac{L_1}{(1-\rho)B\Omega_1}} - 1}{b\gamma_0\left[a-(1-a)\left(2^{\frac{L_1}{(1-\rho)B\Omega_1}}-1\right)\right]}$; $\beta_2 = \frac{2^{\frac{L_2}{(1-\rho)B\Omega_2}}-1}{(1-a)b\gamma_0}$; $\Omega_1 = (1-\rho)T - \frac{\delta_1 L_1}{f_1}$; $\Omega_2 = (1-\rho)T - \frac{\delta_2 L_2}{f_2}$; *and* $x_q = \cos\left(\frac{2q-1}{2Q}\pi\right)$; $t_q = \frac{(x_q+1)}{2} e^{-\sqrt{\beta_1}}$ *and* Q *is the trade-off coefficient between complexity and precision.*

Proof. See appendix A.

To refer to the NOMA-MEC protocol, we propose the second operating protocol system, named OMA-MEC, as follows:

Phase 1- Energy Harvesting Phase: The system works entirely similar to the NOMA-MEC protocol described above, i.e., U receives energy from HAP.

Phase 2- Offloading Phase: The task (L-bits) is offloaded to the MEC server located at the HAP in this phase. In other words, the downlink OMA scheme is applied to offload workload. Accordingly, the received signal at HAP has the form:

$$y_{HAP}^{OMA-MEC} = h_1 x_1 \sqrt{P_t^{OMA}} + n_1, \tag{19}$$

where $P_t^{OMA} = \frac{E_U}{(1-\rho)T-\tau_2^{OMA}} = b^{OMA}P_0 g_1$; $b^{OMA} \triangleq \frac{\eta\rho T}{(1-\rho)T-\tau_2^{OMA}}$; $\tau_2^{OMA} = \frac{\delta_1 L}{f_1}$.

Phase 3- Calculation Phase: The SNR at the HAP to decode the signal is as follow:

$$\gamma_1^{OMA} = \frac{P_t^{OMA}|h_1|^2}{N_0} = b^{OMA}\gamma_0 {g_1}^2, \tag{20}$$

Phase 4- Result Feedback Phase: In this phase, U receives calculation results from HAP for the rest of the time.

Accordingly, we state Theorem 2, describing the system SCP of the OMA-MEC protocol as follow.

Theorem 2. *The exact close-form expression of the SCP of the proposed system under OMA-MEC protocol, denoted by Φ_s^{OMA} over Rayleigh fading channel is as follow:*

$$\begin{aligned} \Phi_s^{OMA} &= \Pr(\tau_1^{OMA} + \tau_2^{OMA} \leq (1-\rho)T) \\ &= e^{-\frac{\sqrt{\beta_3}}{\lambda_1}}, \end{aligned} \tag{21}$$

where $\beta_3 = \frac{2^{\frac{L}{(1-\rho)B\Omega_3}}-1}{b^{OMA}\gamma_0}$; $\Omega_3 = (1-\rho)T - \frac{\delta_1 L}{f_1}$; $\tau_1^{OMA} = \frac{L}{C^{OMA}}$; $C^{OMA} = \frac{L}{(1-\rho)B\log_2(1+b^{OMA}\gamma_0 {g_1}^2)}$.

Proof. See appendix B.

4 Numerical Results and Discussion

In this section, we present the numerical results of the SCP of the proposed system. We use the Monte Carlo simulation method and the Matlab tool to drive simulations and evaluate the correctness of the system analysis. At the same time, the system behavior is investigated under NOMA-MEC and OMA-MEC protocols according to critical parameters such as signal-to-noise ratio, time-switching ratio, power allocation coefficient, and task division ratio. The parameters used in the detailed simulation are shown in Table 1 [14].

In the first experiment, we compared the SCP system under NOMA-MEC and OMA-MEC protocols, as Fig. 3. The SCP curves for the two protocols show similar upward or downward trends. However, it is easy to see that the SCP when the system uses the NOMA-MEC protocol is always higher than the OMA-MEC. This result was investigated when setting the computing capability of the two MEC servers to be the same. Accordingly, the task offloaded for two MECs in the NOMA-MEC protocol will have a shorter execution time than the case of using only one HAP in the OMA-MEC protocol. We conclude that the proposed NOMA-MEC protocol helps the system perform better than the OMA-MEC protocol. This result is repeated when performing investigations with different parameters; therefore, we only evaluate system performance under the NOMA-MEC protocol in subsequent experiments.

Table 1. Simulation Parameters.

Parameters	Notation	Typical Values
Environment		Rayleigh
Transmit power	P_0	$-10 \rightarrow 30$ dB
Time switching ratio	ρ	0.4
CPU-cycle frequency of MEC server deployed in HAP	f_1	10 GHz
CPU-cycle frequency of MEC server deployed in AP	f_2	10 GHz
Channel bandwidth	B	100 MHz
The threshold of latency	T	0.5 s
The number of data bits offloaded to HAP	L_1	0.6 Mbits
The number of data bits offloaded to AP	L_2	0.6 Mbits
Power allocation coefficient	a	0.7
Energy conversion factor	η	0.75

Figure 4 examines the SCP of the system according to the transmitted power with the power allocation coefficient values of 0.6, 0.75, and 0.9, respectively. In all three cases, the descriptive curve Φ_s shows that the larger the transmit power, the better the system performance. This is entirely consistent with formulas (7), (8), and (9); that is, when the transmit power increases, the average transmit SNR increases, leading to an increase in the SINR and SNR values at the HAP and AP, thereby improving the SCP of the system. One note is that with significant transmit power levels (>20 dB), Φ_s reaches saturation value. Therefore, there should be a consideration during system design to ensure system performance at a reasonable energy cost.

Figure 5 depicts the SCP of the system according to the power allocation coefficient with different task division ratios. In which the task division ratio is denoted by ε, $\varepsilon = \frac{L_1}{L}$. Based on the similar form of all three different ε cases, we conclude that there exists an optimal power allocation coefficient (a^*) such that the system performance stands at the maximum. Indeed, Φ_s has a small value when a is small; then Φ_s gradually increases to a maximum value as a increases; and finally, Φ_s tends to decrease as a increase to 1. It shows that the system performance depends essentially on a. Therefore when designing the system, it is necessary to design suitable optimization algorithms so that a^* can be determined to optimize the SCP. Furthermore, there exists a unique point on the graph, which we call the transition point (TP), which has the coordinate a_{TP}. For the values a, which are smaller than a_{TP}, lower ε leads to higher Φ_s. Conversely, when a is larger than a_{TP}, the higher ε is, the better the system performance is.

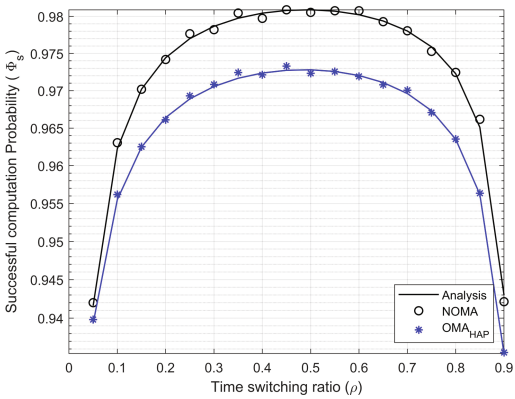

Fig. 3. System performance comparison under the NOMA-MEC and OMA-MEC protocols.

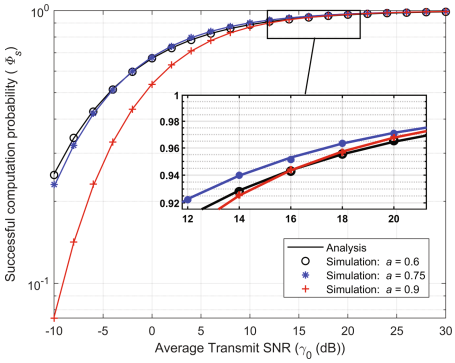

Fig. 4. SCP vs. the average transmit SNR with different power allocation coefficients.

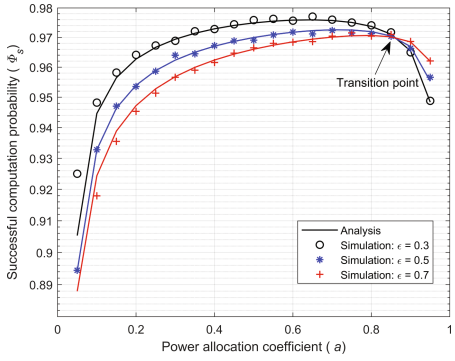

Fig. 5. SCP vs. the power allocation coefficient with different task division ratios.

Figure 6 examines the SCP of the system according to the task division ratio and the time switching ratio. In all three survey cases, when ε increases from 0.05 to 0.95, i.e., the L_1 task length increases and L_2 task length decreases, the system performance degrades from 1% to 2%. Another remark is that an extreme value of Φ_s exists according to the time switching ratio because Φ_s at $\rho = 0.4$ is better than the two cases $\rho = 0.1$ and $\rho = 0.7$.

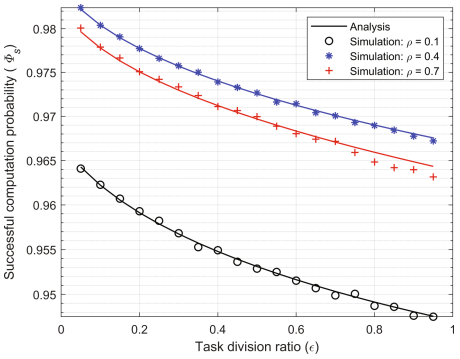

Fig. 6. SCP vs. the task division ratio with different time switching ratios.

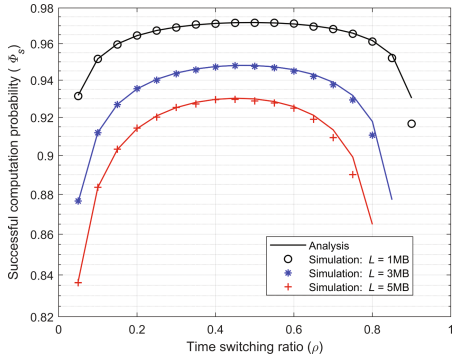

Fig. 7. SCP vs. the time switching ratio with different the task lengths.

Figure 7 examines the SCP of the system according to the time switching ratio with different task sizes. Specifically, when ρ is low, Φ_s is low. When ρ increases to the optimal value (ρ^*), Φ_s reaches its maximum value. When $\rho > \rho^*$, Φ_s tends to decrease. It is imaginable because when ρ is small ($\rho < 0.2$), the time spent in the energy-harvesting phase is narrow, resulting in a low transmit power of U. Thus, the SCP of the system will be low. Meanwhile, when ρ is large ($\rho > 0.8$),

although the transmit power of U is significant, the time spent on offloading and calculation phases is deficient, resulting in a low value of Φ_s. Therefore, designing the system with the optimal time-switching ratio is essential for maximum system performance. Another observation is that task length has a significant effect on system performance. When L increases from 1 MB to 5 MB, the system performance degrades by approximately 10%. Therefore, designing the task of appropriate length in MEC-based networks is one of the basic requirements to ensure system performance.

The simulation results (Simulation) and analytical calculations (Analysis) are consistent in the above experiments, showing our research's correctness.

5 Conclusion

In this paper, we have investigated the system performance of a MEC network that harvests radio energy using NOMA and two access points. One of these two APs is the HAP, and the other is the standard AP. We propose the NOMA-MEC protocol for this network and derive a closed-form expression for the system SCP. To evaluate the NOMA-MEC protocol, we compare it with the OMA-MEC protocol. The results show the superiority of our approach. We used Monte Carlo simulation to verify the correctness of the mathematical analysis results and investigate the system's performance through critical parameters such as transmit power, time switching ratio, power allocation coefficient, and task division ratio. The results show that the performance of the proposed system depends on the main parameters mentioned above. To improve the system performance, we can determine one of the methods: (i) increase the transmit power, (ii) select the optimal time switching ratio, power allocation coefficient, and task division ratio. We will propose an algorithm to find these optimal coefficients in future work.

Acknowledgment. This research is funded by Vietnam National Foundation for Science and Technology Development (NAFOSTED) under grant number 102.04-2021.11.

APPENDIX A: PROOF OF THEOREM 1

In this section, we prove Theorem 1. From the fomular (12) to (14), and (17), we rewrite the SCP of the proposed system as follows:

$$
\begin{aligned}
\Phi_s^{NOMA} &= \Pr\left(\frac{L_1}{C_1}+\frac{\delta_1 L_1}{f_1} \le (1-\rho)\,T, \quad \frac{L_2}{C_2}+\frac{\delta_2 L_2}{f_2} \le (1-\rho)\,T\right) \\
&= \Pr\left((1-\rho)\,B\log_2\left[1+\frac{ab\gamma_0 g_1^2}{(1-a)b\gamma_0 g_1^2+1}\right] \ge \frac{L_1}{\Omega_1},\ (1-\rho)\,B\log_2\left[1+(1-a)b\gamma_0 g_1 g_2\right] \ge \frac{L_2}{\Omega_2}\right) \\
&= \Pr\left(\frac{ab\gamma_0 g_1^2}{(1-a)b\gamma_0 g_1^2+1} \ge 2^{\frac{L_1}{\Omega_1(1-\rho)B}}-1,\ (1-a)b\gamma_0 g_1 g_2 \ge 2^{\frac{L_2}{\Omega_2(1-\rho)B}}-1\right) \\
&= \begin{cases} 0, & \text{if } \frac{a}{1-a} \le 2^{\frac{L_1}{(1-\rho)B\Omega_1}}-1 \\ \Pr\left(g_1 \ge \sqrt{\beta_1}, g_2 \ge \frac{\beta_2}{g_1}\right), & \text{if } \frac{a}{1-a} > 2^{\frac{L_1}{(1-\rho)B\Omega_1}}-1 \end{cases} \\
&= \begin{cases} 0, & \text{if } \frac{a}{1-a} \le 2^{\frac{L_1}{(1-\rho)B\Omega_1}}-1 \\ \underbrace{\int\limits_{\sqrt{\beta_1}}^{\infty}\left[1-F_{g_2}\left(\frac{\beta_2}{x}\right)\right]f_{g_1}(x)dx}_{I}, & \text{if } \frac{a}{1-a} > 2^{\frac{L_1}{(1-\rho)B\Omega_1}}-1 \end{cases}
\end{aligned}
\tag{22}
$$

We focus on the case $\frac{a}{1-a} > 2^{\frac{L_1}{(1-\rho)B\Omega_1}}-1$. The integral I is calculated as:

$$
\begin{aligned}
I &= \int\limits_{\sqrt{\beta_1}}^{\infty}\left[1-F_{g_2}\left(\frac{\beta_2}{x}\right)\right]f_{g_1}(x)dx \\
&= \frac{1}{\lambda_1}\int\limits_{\sqrt{\beta_1}}^{\infty} e^{-\frac{x}{\lambda_1}-\frac{\beta_2}{\lambda_2 x}}dx \\
&\overset{(*)}{=} \frac{1}{\lambda_1}\int\limits_{0}^{e^{-\sqrt{\beta_1}}} t^{\frac{1}{\lambda_1}-1}e^{\frac{\beta_2}{\lambda_2 \ln t}}dt \\
&\overset{(**)}{=} \frac{\pi e^{-\sqrt{\beta_1}}}{2Q\lambda_1}\sum_{q=1}^{Q} t_q^{\frac{1}{\lambda_1}-1}e^{\frac{\beta_2}{\lambda_2 \ln t_q}}\sqrt{1-x_q^2}.
\end{aligned}
\tag{23}
$$

where step (*) is obtained by putting $t = e^{-x}$. The step (**) is achieved by applying the Gauss-Chebyshev quadrature approximation. Here, Theorem 1 has been proved.

APPENDIX B: PROOF OF THEOREM 2

We continue to demonstrate Theorem 2 in this section. From the definition formula, Φ_s^{OMA} is implemented as follows:

$$\begin{aligned}
\Phi_s^{OMA} &= \Pr\left(\frac{L}{(1-\rho)B\log_2(1+b^{OMA}\gamma_0 {g_1}^2)} + \frac{\delta_1 L}{f_1} \le (1-\rho)T\right) \\
&= \Pr\left(\frac{L}{(1-\rho)B\log_2(1+b^{OMA}\gamma_0 {g_1}^2)} \le \underbrace{(1-\rho)T - \frac{\delta_1 L}{f_1}}_{\Omega_3}\right) \\
&= \Pr\left(\underbrace{\frac{2^{\frac{L}{(1-\rho)B\Omega_3}}-1}{b\gamma_0}}_{\beta_3} \le {g_1}^2\right) \\
&= 1 - F_{g_1}(\sqrt{\beta_3}) \\
&= e^{-\frac{\sqrt{\beta_3}}{\lambda_1}}
\end{aligned} \tag{24}$$

We have completed the proof of Theorem 2.

References

1. Zhou, Y., Zhang, D., Xiong, N.: Post-cloud computing paradigms: a survey and comparison. Tsinghua Sci. Technol. **22**(6), 714–732. https://doi.org/10.23919/TST.2017.8195353
2. Hou, X., Ren, Z., Yang, K., Chen, C., Zhang, H., Xiao, Y.: IIoT-MEC: a novel mobile edge computing framework for 5G-enabled IIoT. In: Proceedings 2019 IEEE Wireless Communications and Networking Conference (WCNC), pp. 1–7 (2019). https://doi.org/10.1109/WCNC.2019.8885703
3. Ma, H., Li, S., Zhang, E., Lv, Z., Hu, J., Wei, X.: Cooperative autonomous driving oriented MEC-aided 5G–V2X: prototype system design, field tests and AI-based optimization tools. IEEE Access **8**, 54288–54302 (2020). https://doi.org/10.1109/ACCESS.2020.2981463
4. Mao, Y., You, C., Zhang, J., Huang, K., Letaief, K.B.: A survey on mobile edge computing: the communication perspective. IEEE Commun. Surveys Tut. **19**(4), 2322–2358 (2017)
5. Mach, P., Becvar, Z.: Mobile edge computing: a survey on architecture and computation offloading. IEEE Commun. Surveys Tut. **19**(3), 1628–1656 (2017)
6. Mehrabi, M., You, D., Latzko, V., Salah, H., Reisslein, M., Fitzek, F.H.P.: Device-enhanced MEC: multi-access edge computing (MEC) aided by end device computation and caching: a survey. IEEE Access **7**, 166079–166108 (2019). https://doi.org/10.1109/ACCESS.2019.2953172
7. Truong, T.P., Nguyen, T.V., Noh, W., Cho, S., et al.: Partial computation offloading in NOMA-assisted mobile-edge computing systems using deep reinforcement learning. IEEE Internet Things J. **8**(17), 13196–13208 (2021)

8. Ha, D.-B., Truong, V.-T., Ha, D.-H.: A novel secure protocol for mobile edge computing network applied downlink NOMA. In: Vo, N.-S., Hoang, V.-P. (eds.) INISCOM 2020. LNICST, vol. 334, pp. 324–336. Springer, Cham (2020). https://doi.org/10.1007/978-3-030-63083-6_25
9. Nguyen, M.T., Tran, H.T., Nguyen, C.V., Ala, G., Viola, F., Colak, I.: A novel framework of hybrid harvesting mechanisms for remote sensing devices. In: 2022 IEEE 21st Mediterranean Electrotechnical Conference (MELECON) (IEEE), pp. 1007–1012 (2022)
10. Truong, V.-T., Vo, M.-T., Ha, D.-B.: Performance analysis of mobile edge computing network applied uplink NOMA with RF energy harvesting. In: Vo, N.-S., Hoang, V.-P., Vien, Q.-T. (eds.) INISCOM 2021. LNICST, vol. 379, pp. 57–72. Springer, Cham (2021). https://doi.org/10.1007/978-3-030-77424-0_6
11. Nguyen, M.T., Nguyen, C.V., Tran, H.T., Viola, F.: Energy harvesting for mobile agents supporting wireless sensor networks. Energy Harvesting Syst. (2022)
12. Truong, V.T., Ha, D.B.: Secured scheme for RF energy harvesting mobile edge computing networks based on NOMA and access point selection. In: Proceedings 2020 7th NAFOSTED Conference on Information and Computer Science (NICS), pp. 7–12 (2020). https://doi.org/10.1109/NICS51282.2020.9335833
13. Zhu, B., Chi, K., Liu, J., Yu, K., Mumtaz, S.: Efficient offloading for minimizing task computation delay of NOMA-based multiaccess edge computing. IEEE Trans. Commun. **70**(5), 3186–3203 (2022)
14. Truong, V.T., Ha, D.B., So-In, C., et al.: On the system performance of mobile edge computing in an uplink NOMA WSN with a multiantenna access point over Nakagami-m fading. IEEE/CAA J. Automatica Sinica **9**(4), 668–685 (2022)